A computer vision approach to analyse and classify tool wear level in milling processes using shape descriptors and machine learning techniques

A computer vision approach to analyse and classify tool wear level in milling processes using shape descriptors and machine learning techniques

María Teresa García-Ordás [*1], Enrique Alegre [†1], Víctor González-Castro [‡2], and Rocío Alaiz-Rodríguez [§1]

[1]University of León
[2]University of Edinburgh

Abstract

In this paper we present a new approach to categorize the wear of cutting tools used in edge profile milling processes. It is based on machine learning and computer vision techniques, specifically using B-ORCHIZ, a novel shape based descriptor computed from the wear region image. A new Insert dataset with 212 images of tool wear has been created to evaluate our approach. It contains two subsets: one with images of the main cutting edge, and the other one with the edges that converge to it (called Insert-C and Insert-I, respectively). The experiments were conducted trying to discriminate between two (Low-High) and three (Low-Medium-High) different wear levels and the classification stage was carried out using a Support Vector Machine (SVM). Results show that B-ORCHIZ outperforms other shape descriptors (aZIBO and ZMEG) achieving accuracy values between 80.24% and 88.46% in the different scenarios evaluated. Moreover, a hierarchical cluster analysis was performed, offering prototype images for wear levels, which may help researchers and technicians to understand how the wear process evolves. These results show a very promising opportunity for wear monitoring automation in edge profile milling processes.

Keywords— Tool wear classification, B-ORCHIZ, aZIBO, ZMEG, shape description

[*]e-mail: mgaro@unileon.es; Corresponding Author
[†]e-mail: ealeg@unileon.es
[‡]e-mail: victor.gonzalez@ed.ac.uk
[§]e-mail: rocio.alaiz@unileon.es

1 Introduction

Optimizing tool replacement operations may produce a significant improvement in manufacturing efficiency and competitiveness. Conservative approaches usually replace the tools before it is actually necessary in order to avoid the high cost of tool failure, so they still have some lifetime. In [1], it is estimated that cutting tool failures typically represent a 20% of the time a machine is inactive. However, replacing tools at the right moment is essential, not only because of the cost of cutting tools themselves, but also for the indirect costs due to the unproductive time needed to carry out the tool replacement. For this reason, tool condition monitoring has become a key point in industry for optimizing operations and increase productivity. This work addresses the task of tool wear monitoring in edge profile milling processes using computer vision and machine learning techniques.

Approaches to tool wear monitoring proposed so far fall into two broad categories: indirect and direct methods. Indirect monitoring methods estimate the wear by measuring variables such as cutting forces [2, 3, 4], vibration [5, 6] or acoustic emission [7], that are somehow correlated to tool wear stages. However, the relationship between tool wear and the observed variables depends on the cutting conditions which, in general, are not known in advance. Although these methods are the most popular, the precision achieved with them can be seriously affected by noise signals in industrial environments.

In contrast, direct methods - usually based on computer vision systems - have the advantage of measuring actual geometric changes in the tool, offering more accuracy and reliability [8]. A review of machine vision sensors for tool condition monitoring is presented in [9, 10]. Zhang et al. [11] propose an online system for wear measurement in ball-end milling processes, where the wear area is accurately measured by finding its edges. A computer vision technique is presented in [12] to calculate the tool area based on the drill image thresholding, helping to select optimal drilling parameters in relation to tool wear. Datta et al. propose a method [13] based on texture analysis and Voronoi tessellation to measure progressive tool wear. A method for on-machine tool progressive monitoring of tool flank wear by processing the turned surface images in micro-scale is presented by Dutta et al. [14]. In this case, micro-scale analysis of turned surface is performed using also texture analysis, in particular, discrete wavelet transform.

Recently, the computer vision research community has successfully developed new methods which use shape information in order to describe the images [15, 16]. These shape features are extracted from the images and later on processed by a classification or regression model to provide relevant information of the tool wear status. Shape description methods have already been applied in the tool wear monitoring field to ensure the optimal replacement of the tool in lathe processes and they propose the use of Hu and Legendre moments [17].

Our problem is quite different from that of [17] in the sense that we determine the tool wear in edge profile milling processes instead of lathe processes. In milling, the wear shape is distributed uniformly along the insert while in lathe

processes the wear occurs on the same area concavely. Also, most works that deal with milling focus on end milling or face milling. Thus, monitoring tool wear in edge profile milling processes states a more challenging task since the insert distribution is not typical and the head geometry is more complex.

In this paper we present B-ORCHIZ, a new shape descriptor based on the boundary point description. This method combines global and local shape descriptors, which improves the characterization of the images [18, 19, 20]. We evaluate it on an image-based tool wear monitoring system for edge profile milling. Its accuracy using a SVM classifier to determine the wear level is compared with aZIBO [21] and with ZMEG [19], that also use local and global features.

Additionally, a cluster analysis allows to study the shape descriptor capacity (a) to cluster insert images into homogeneous groups and (b) to provide prototype images for certain tool wear stages with the goal of visualizing where and how the wear takes place and how the typical wear shape is. This last shape analysis allows to improve the comprehension of the wear level classification and to help human experts to distinguish among them, demonstrating that the shape of the wear can be used to determine whether the insert is intact, softly damaged or highly damaged.

It should be pointed out that tool wear monitoring proposals often involve expensive sensors and machines such as the work in [22], with interesting results, but the cost of all machines, including different microscopes, is higher than $20.000 in the cheapest scenario. In [23], just the system for roughness surface measurement is approximately $2000. Our proposal aims at combining low cost devices and fast software techniques that allow to evaluate the tool wear status in just a few seconds. It requires a simple Genie M1280 camera under $500 to take grayscale images and three led bars to avoid undesirable brights and shadows.

The paper is organized as follows: Section 2 states the shape description problem and presents the novel descriptor B-ORCHIZ. Section 3 describes the Insert dataset and how it was acquired. The system accuracy is assessed in Section 4 and compared with an approach based on the region wear size in Section 5. Afterwards, in Section 6 the descriptors are evaluated using a clustering algorithm and in Section 7, we show the representative images for each wear level. Finally, the conclusions are discussed in Section 8.

2 The B-ORCHIZ proposal for shape description

In order to characterize the tool wear, we propose to use shape descriptors computed from the tool image. In particular, the combination of global and local shape descriptors is considered to be quite reliable and has been extensively applied lately [18, 19, 20]. On the one hand, local descriptors are used to characterize small patches of the image. On the other hand, global descriptors

provide comprehensive information of the whole image. However, they are not as robust as local ones because they are not sensitive to changes in small parts of the image.

One example is the work carried out by Singh et al. [18], that combines the Angular Radial Transform as global descriptor and Polar Hough Transform as local one. Anuar et al. propose ZMEG [19], which is also a fusion of global and local descriptors but, in this case, they employ Zernike moments and Edge Gradient Co-occurrence Matrix (EGCM), respectively. Later, García-Ordás et al. introduce aZIBO [21], which used Zernike moments as a global descriptor and the EGCM as local one, but extended it, making it invariant to rotation.

In this section, we present a novel shape descriptor, called B-ORCHIZ, which also combines global and local descriptors. Additionally, we describe a way to make it rotationally invariant.

2.1 Global Shape Description

Global Shape information is described using Zernike moments (specifically the module of the first 36 coefficients, up to the tenth order) in the same way as the work carried out by Anuar et al. in ZMEG [19] . However, in our case we use the images with intensity values between 0 and 255 (not binary ones) and resize them to 128×128 to give more information to the Zernike moments coefficients thanks to the interpolation process which generates a grey-scale image, not just a binary one [21]. It is well known that the module of the Zernike moments of an image f has the property of being invariant to rotation.

2.2 Local Description

B-ORCHIZ uses the Invariant Boundary Descriptor (IBD) - a fusion of the IEGCM and the Boundary Orientations Chain (BOC) - as local shape descriptor. IEGCM is an invariant variation of EGCM proposed in [19]. Original EGCM is obtained as follows: First of all, the boundary points of the image are obtained. In this case, the edge detector proposed by Belongie et al. [24] which yields a uniformly spaced sample of the points was used. The result of this process is shown in Fig. 1.

The set of boundary points is represented as:

$$P = \{(x_i, y_i) \in \mathbb{R}^2 \ : \ 1 \leq i \leq m\},$$

where m is the number of boundary points.

In the second step, the gradient of each boundary point in P is calculated by means of Eq.(1).

$$O(x, y) = \arctan\left(\frac{I(x+1, y) - I(x-1, y)}{I(x, y+1) - I(x, y-1)}\right), \tag{1}$$

where x and y are the image coordinates.

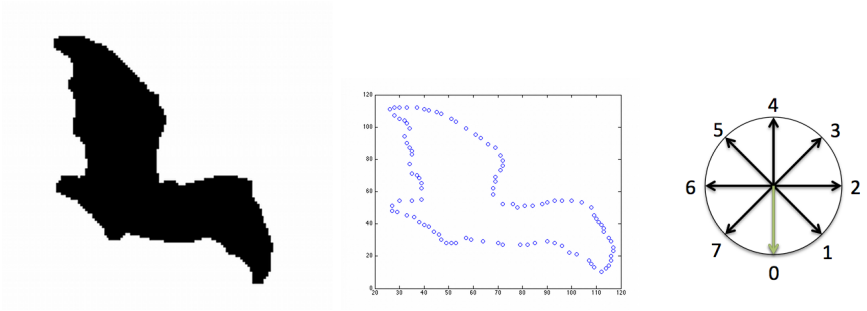

(a) (b) (c)

Figure 1: (a) Original image, (b) its boundary points and (c) the eight quantized orientations.

These gradient orientations are discretized into the eight values shown in Fig. 1(c).

In the third step, the EGCM is built taking into account only the points among its eight neighbors which are part of the boundary. Fig. 2 depicts the EGCM construction for a boundary point.

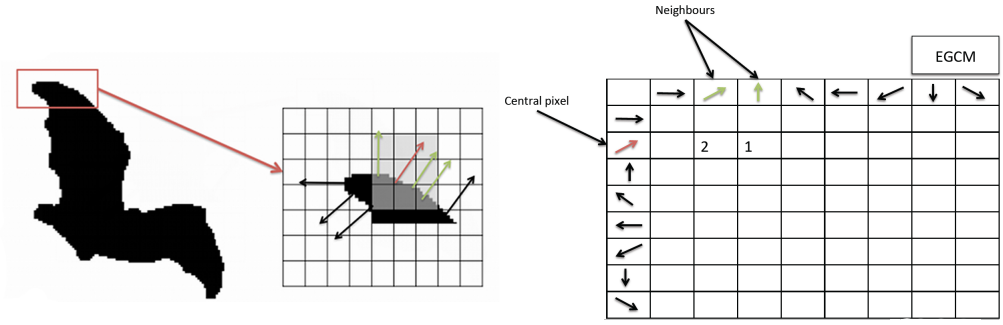

Figure 2: Example of the orientations taken into account for the boundary point shown in red for the composition of the EGCM (left). Example of the composition of the edge gradient co-occurrence matrix taking into account the boundary point shown in this figure (right).

Finally, the eight rows of the EGCM are concatenated yielding a 64-element vector.

The local descriptor IEGCM is proposed in [21] and it made EGCM method rotationally invariant. To do this, the pair of boundary points b_1 and b_2 whose Euclidean distance is the longest is found and then, the angle of vector $\vec{b} = b_1\vec{b}_2$ is calculated by means of Eq.(2). In case there are more than one pair of points with such distance, it is taken the pair (b_1, b_2) for which the segment joining

them, $\overline{b_1 b_2}$, is the nearest to the centroid of the shape. The point b_1 or b_2 with more boundary points in its 21×21 neighborhood is selected as origin. The size of the neighborhood has been determined experimentally. The gradient orientation of the origin, ϕ_d, is placed at the first row and column in the edge gradient co-occurrence matrix and the rest of orientations are shifted following their original position. Therefore, if EGCM is $[\phi_1, \phi_2, \ldots, \phi_d, \ldots, \phi_8]$, then IEGCM(rotationally invariant version of EGCM) is $[\phi_d, \ldots, \phi_8, \phi_1, \ldots, \phi_{d-1}]$.

$$\alpha_{\vec{b}} = \arctan\left(\frac{b_2(2) - b_1(2)}{b_2(1) - b_1(1)}\right), \tag{2}$$

An example of this process is shown in Fig. 3, where the same matrix is obtained for the same image in two different orientations.

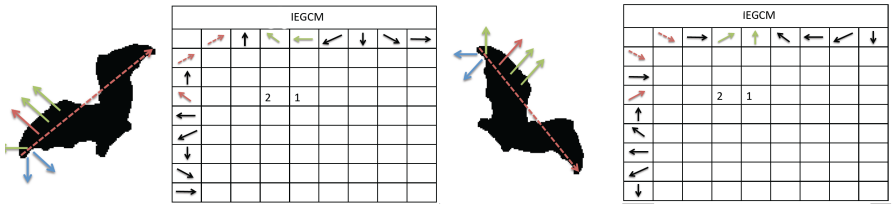

Figure 3: Example of the invariance to rotation of the IEGCM. Red dotted line represents the orientation between the furthest points in the boundary. The red arrow corresponds to the gradient orientation of the point whose IEGCM is calculated. The green arrows are taken into account (because they are located inside the neighborhood) whereas the blue arrows represent points that are not in the influence area of the selected one.

Finally, the eight rows of the IEGCM are concatenated yielding a 64-element vector. Unlike the work in [19] where these descriptor values were normalized in the range of 0 to 1, in this work we preserve the original values in order to obtain as much information as possible.

Next, we present the second local descriptor, the boundary orientations chain (BOC). It is a vector whose elements are the orientations of the m boundary points. In order to achieve invariance to rotation, the first element must be determined. The first step is to find the two furthest contour points b_1 and b_2, which is done following the same process as it was done to find the first orientation in the IEGCM. The selected point b_1 or b_2 will be the one with more boundary points in its 21×21 neighborhood. Thereafter, the orientation values are normalized to achieve invariance to rotation so the first orientation, whatever it is, is considered as the value 0 in the chain and the rest are shifted according to it, as is shown in Fig. 4.

After that, the rotationally invariant descriptor is the vector of m elements representing the orientation of each boundary point. In this work, the local descriptor IBD is the concatenation of the previous IEGCM and the BOC. After all this process, the global and local descriptors are concatenated.

Figure 4: Example of the Boundary Orientations Chain (BOC) rotation invariance. The red arrow represents the maximal distance between points in the contour of the image. The green arrow is the orientation of the first point of the chain. The values assigned to each orientation are shifted locating the green arrow in the top of the diagram (value 0).

3 Insert Dataset

The aim of this work is to characterize the insert state based on the wear region shape. For this purpose, we have acquired an Insert dataset processing the images of 53 tools as the ones shown in Fig. 5.

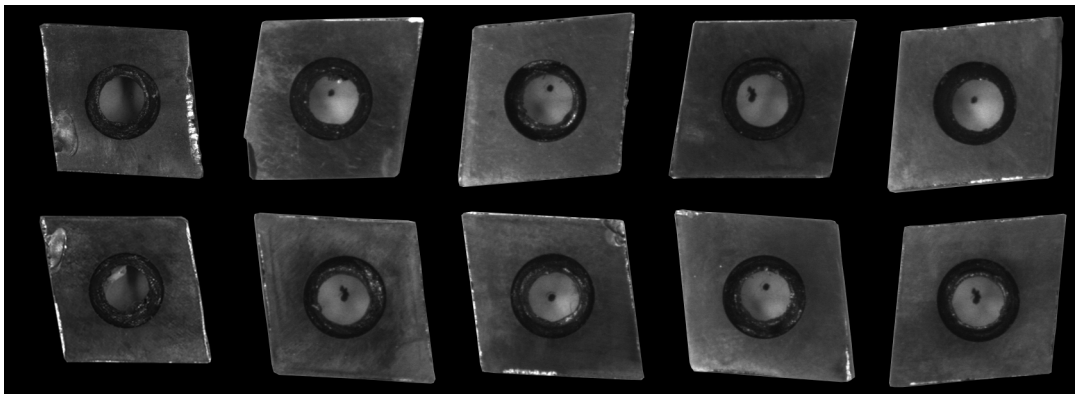

Figure 5: Insert dataset example. Inserts on the left present high wear while inserts on the right present low wear taking into account the left cutting edge.

Using grayscale images, instead of 3D images, we are able to reduce the time to measure the wear, what makes feasible the deployment of our proposal in a real environment.

The images were captured using a monochrome camera, model Genie M1280 1/3" with a $25mm$ optic AZURE. The focus and aperture are manual. The sensor has a resolution of 1280×960 pixels. The monochrome camera and its specifications are shown in Fig. 6 and in Table 1.

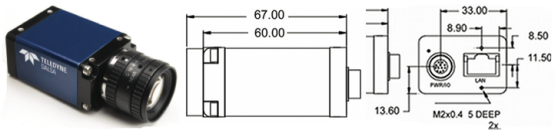

Figure 6: Genie M1280 (left side), lateral view (center image), back view (right side).

Table 1: Genie M1280 specifications.

	Camera Specifications
Active Resolution	1280 x 960
Frame Rate	24fps
Exposure Control	Programable, or via External Trigger
Output	Gigabit Ethernet, also support 100 Mbps (RJ-45)
Lens Mount	C or CS-mount / Right Angle available
Size	44mm x 29mm x 67mm (including lens adapter)
Power Supply	12 to 24 v (4 W)

In order to improve the contrast in black and white images, we used two lighting bars of red LEDs (BDBL-R8216H). Images have been taken on the inserts dismounted from the cutting head and placed on an uniform background.

To acquire the images, a prototype in which the camera was placed in a support with adjustable distance, was constructed. This prototype and also the lighting system are shown in Fig. 7.

The goal is to assess the wear level in each wear region so two preprocessing steps were carried out: The cropping of cutting edges (section 3.1) and the wear region extraction (section 3.2).

3.1 Cropping of cutting edges

Each insert, captured as a grayscale image and with a masked background (Fig. 8 (a)) is subjected to a pre-processing step that yields four new images, one for each of the four cutting edges of the insert. Therefore, we crop each cutting edge and rotate the two vertical ones, obtaining four images with a horizontal

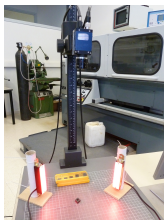

Figure 7: Image capture prototype. The support in which the camera is placed and the LEDs bars employed are shown.

cutting edge on it, for each insert processed. In this section, this pre-processing step is explained.

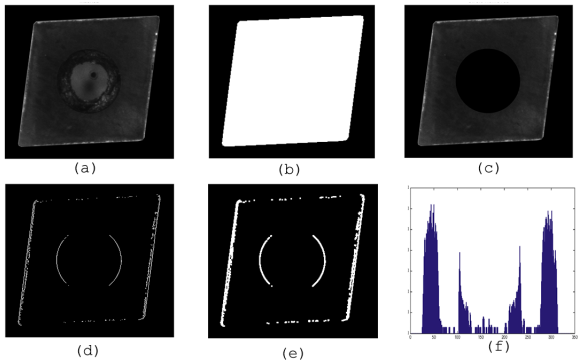

Figure 8: (a) Masked image of an insert. (b) Binary image after applying a threshold of 0.01. (c) Image with the center circle removed. (d) Image after Sobel filter convolution. (e) Image after applying morphological operations (dilatation, opening). (f) Vertical projection of (e) to identify the edges.

First of all, the central portion of the insert is removed (Fig. 8 (c)), masking out a circular region, so we first need to locate its center and obtain the length of its radius. To determine the circle center, the image is binarized in order to remove the background, using a threshold of 0.01 - obtained empirically -, so the pixels of the insert area are set to 1 and the background to 0 (Fig. 8 (b)). The centroid of this area will be considered as the center of the central circle (x_c, y_c), where x_c and y_c are the mean value of all the x and y coordinate pixels with value 1, respectively. The radius of the circle R_c is considered to be $R_c = D/4.92$, where D is the length of the major diagonal of the insert and the ratio value, 4.92, was obtained taking into account previous knowledge of the size of the central circle respect the insert, which is the same in all the samples.

Thereafter, four regions with a width of one sixth of the insert and the same height, which contains the corresponding four cutting edges of the insert are extracted. We only explain how the west edge is extracted; the other three edges -north, east and south- are extracted using the same procedure rotating the original image 90°, 180° and 270°, respectively. Using the gray-scale image resulting from the previous step, a vertical Sobel filter with a kernel of 3x3 is applied to detect the inserts contours (Fig. 8 (d)). These contours are then dilated and opened using a structuring element with square shape of size 3 (Fig. 8 (e)), and vertically projected onto the horizontal axis (Fig. 8 (f)). The first non-zero element in this projection indicates the x coordinate where the cutting edge starts. Then, the image of the region is cropped from the starting x position with a width of 100 pixels and the same height as the original image. A parametric margin of 25 pixels is added to each side in order to increase the

crop area, because experimental tests showed that some inserts lost some edge pixels due to too tight crops.

Since inserts are rhomboid-shaped and their cutting edges are not aligned with the vertical and horizontal axis, the edges images are rotated to make the cutting edges to be aligned with the horizontal axis. To carry out this operation, a horizontal Sobel filter (3x3 kernel) followed by a morphological dilation is applied with the same structuring element used in the previous step. The resulting image is filtered to remove smaller objects leaving a binary image containing only the cutting edge. Finally, the orientation of the major axis of an ellipse that contains the edge is estimated, so the edge is rotated to compensate this orientation and leave it in horizontal position. Some examples of the cropping of cutting edges can be seen in Fig. 9.

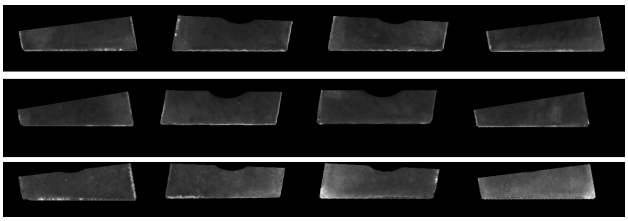

Figure 9: Rotated crops example.

3.2 Wear regions extraction

Once we have obtained the regions with the edge information, the next step consists of extracting the wear within each image. In our case, it is more important a correct wear shape segmentation that an automatic one due to the need of having accurate shape information, so a manual ground truth of the wear region was segmentated. At the end of this process, we got a dataset composed by 212 binary images. An example of the edges dataset is shown in Fig. 10.

Figure 10: This is an example of the obtained dataset for the images shown in Fig. 5. Each of the previous insert gray-scale images with masked background follow a preprocessing step that yields four new images, one for each cutting edge in horizontal position.

Cropped images are usually formed by two different types of wear regions:

Complete and incomplete regions. The complete regions correspond with the horizontal cutting edge in the crop, and the incomplete regions represent the edges that converge in the complete one. To determine the wear of the complete edge by itself and also how it is influenced by the incomplete edges, we divided the whole Insert dataset into two: (a) Insert-C subset with the complete edges that correspond with the horizontal wear in the cropped images, and (b) Insert-I subset with the incomplete ones which orientations are vertical in the images. An example is shown in Fig. 11.

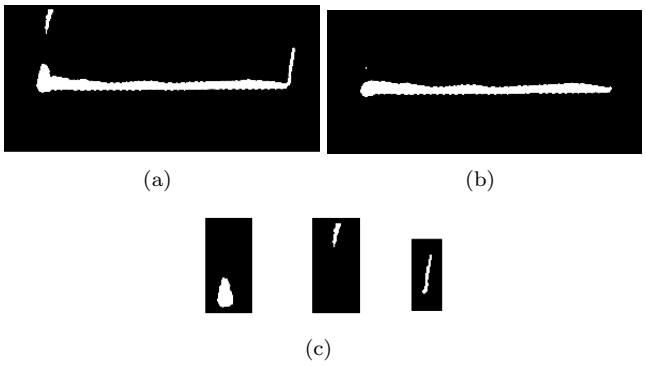

Figure 11: (a) The image containing both types of edges: The complete edge placed in horizontal position and the imcompletes edges in vertical position. (b) The complete edge and (c) Incomplete edges from vertical edges of (a).

An expert classified visually all the wear regions included in the dataset to generate the ground truth, carrying out two types of ratings depending on how many wear classes were taken into account: two (i.e., Low wear (L) with 260 images and High wear (H) with 313 images) or three (i.e., Low wear (L) with 126 images, Medium wear (M) with 260 images and High wear (H) with 187 images). The expert carried out the labelling process by means of a visual assessment, relying on his previous knowledge and experience. This task is not easy as it depends on many parameters like the size of the wear area, its location or how deep it is.

In Tables 2 and 3 we can see the mean area (in mm^2) of the wear classification made by the expert and their standard deviation. The measures were carried out for the three datasets and distinguish between two and three wear classes. As we can see, the mean area is higher for the inserts categorized by the expert as high wear. This information resulted very interesting leading us to perform a classification of the wear based on these parameters.

Table 2: Mean area of the wear for the L-H labelling and their standard deviation (mm^2)

	Insert-C	Insert-I
L	27.25± 9.66	4.88± 2.06
H	48.55± 20.29	12.05 ± 6.43

Table 3: Mean area of the wear for the L-M-H labelling and their standard deviation (mm^2)

	Insert-C	Insert-I
L	21.64± 7.53	3.55± 1.47
M	34.72± 9.44	7.43 ± 2.24
H	51.76± 21.63	14.91 ± 7.17

4 Tool Wear Classification Based on the Wear Region Shape

In this section, we evaluate empirically the classification accuracy achieved with previously proposed shape descriptors and compare them with B-ORCHIZ. Both subsets (Insert-C and Insert-I) were evaluated, first separately and later both together in order to study the possible influence of vertical edges into the main cutting edge. In all cases, classification was performed using a Support Vector Machine (SVM) with linear, second order polynomial and intersection kernels. The Least Square algorithm was used as training method. The classification has been carried out using a stratified 10-fold cross validation. Therefore, the whole dataset (i.e. Insert-C, Insert-I or the complete dataset) is partitioned randomly into 10 equally sized subsets with the same distribution as the original dataset. Of the 10 subssets, 9 are used to train the model and the remaining one is used as the test set. The cross validation is repeated 10 times using a different subset each time as test set. The 10 results from the 10 folds are averaged to provide the final result in terms of accuracy, which is calculated as the proportion of true results (both true positives and true negatives) among the total number of cases examined.

For both subsets the classification accuracies obtained by our proposal B-ORCHIZ, aZIBO and ZMEG are shown for the L-H and L-M-H labelling in Tables 4 and 5. Another classification was carried out combining both subsets to determine the influence of the vertical edges on the horizontal ones. The results are shown in Table 6.

For the Insert-C subset (Table 4), B-ORCHIZ and aZIBO achieved an accuracy of 87.02% in the binary classification using the intersection kernel while ZMEG obtained just 85.58%. In the more challenging three-class classification,

the performance of B-ORCHIZ was higher than the other two methods, 81.25%, in contrast with the 76.92% and 76.44% of aZIBO and ZMEG, respectively. It is remarkable that in all the experiments, the intersection kernel has shown the best performance, improving the three-class classification in a 35.19% and a 60.95% with respect to the linear and the polynomial kernels, respectively.

Table 4: Classification Accuracy (in %) using SVM (linear, quadratic and intersection kernels) of the two and three-class scenarios for the Insert-C dataset.

	L-H			L-M-H		
Classifier	B-ORCHIZ	aZIBO	ZMEG	B-ORCHIZ	aZIBO	ZMEG
SVM-Linear	70.77	72.12	73.08	60.10	58.17	58.17
SVM-Quadratic	80.29	75.96	77.88	50.48	49.52	49.04
SVM-Intersection	**87.02**	**87.02**	85.58	**81.25**	76.92	76.44

Table 5: Classification Accuracy (in %) using SVM (linear, quadratic and intersection kernels) of the two and three-class scenarios for the Insert-I dataset.

	L-H			L-M-H		
Classifier	B-ORCHIZ	aZIBO	ZMEG	B-ORCHIZ	aZIBO	ZMEG
SVM-Linear	78.02	76.37	76.65	61.54	70.60	72.25
SVM-Quadratic	76.37	67.58	74.84	61.26	60.16	64.01
SVM-Intersection	**88.46**	84.89	83.52	**82.69**	82.14	79.40

In Fig. 12 we can see some examples of misclassified images. The first column shows some images whose ground truth (ie., provided by the expert) is low wear and have been misclassified as having high wear, whereas in the second column the opposite case is depicted. As we can see, the three examples that actually have low wear are large, even wider than the third image with high wear. It is also noticeable that two of the images misclassified as low wear have a very small wear region, which can be easily confused with a low wear one. As the system works with binary images, it has no possibility to take into account the depth of the wear, which could be one of the reasons for the expert to label them in this way.

In the case of the Insert-I dataset (see Table 5), the behaviour of all the methods is very similar to the previous analysis. In the binary problem, B-ORCHIZ outperforms all the other methods achieving an accuracy of 88.46%: 4.21% and 5.91% higher than aZIBO and ZMEG respectively. In the L-M-H classification, ZMEG and aZIBO obtained hit rates of 79.42% and

Table 6: Classification Accuracy (in %) using SVM (linear, quadratic and intersection kernels) of the two and three-class for the Insert dataset (full dataset).

	L-H			L-M-H		
Classifier	B-ORCHIZ	aZIBO	ZMEG	B-ORCHIZ	aZIBO	ZMEG
SVM-Linear	80.42	78.32	79.90	62.59	63.11	66.96
SVM-Quadratic	81.12	71.33	72.03	72.52	57.69	61.36
SVM-Intersection	**87.06**	84.44	83.74	**80.24**	78.85	75.87

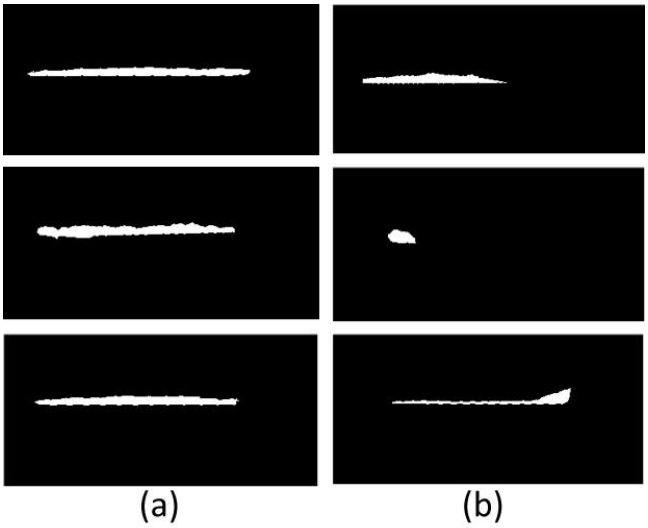

Figure 12: Examples of images: (a) low wear inserts missclassified as high wear and (b) high wear inserts missclassified as low wear.

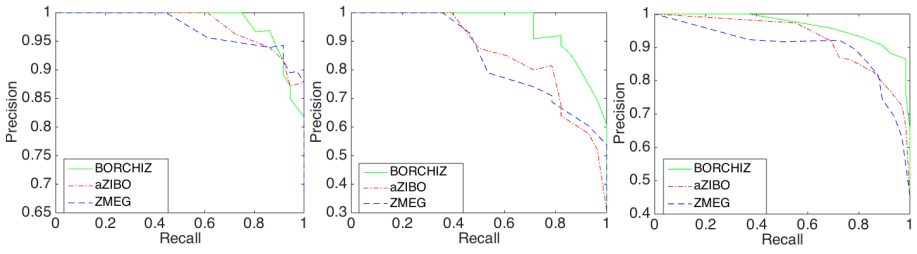

Figure 13: Precision-Recall curves using B-ORCHIZ, aZIBO and ZMEG for Insert-C, Insert-I and the whole Insert dataset (from left to right).

82.14% respectively, while B-ORCHIZ achieved 82.69%. Once again, the best performance was achieved using the intersection kernel in all the tests.

The third experiment consists in using the whole Insert dataset, which is more challenging due to the intra-class variation of the dataset. The aim is to assess the influence of the vertical edges on the final evaluation of the cutting edge. The experiments demonstrated (see Table 6) that in terms of classification accuracy the fusion of both subsets does not improve classification leading to similar results to the Insert-C dataset and slightly worse than the Insert-I dataset.

The precision-recall curves of the classifications using B-ORCHIZ and the other assessed descriptors for Insert-C, Insert-I and the whole Insert dataset are shown in Fig. 13. It can be seen that B-ORCHIZ leads to the best performance for the three scenarios considered.

Results show that combining the complete edge data with the incomplete edge data does not contribute to improve the classification accuracy. On the other hand, the incomplete edge data by itself allows to assess the wear level with a slightly higher accuracy compared to the one achieved with the complete edge data. These results can be explained because for the incomplete edge, all the extracted information is closer to the corners of the inserts, which usually are the places where the wear is shown sooner and stronger. For this reason, using just the information of the corners and avoiding the central part of the cutting edge, the precision of the system increases. In the Precision-Recall curves (Fig. 13) we can also see how the precision decreases faster when both datasets are combined than when they are evaluated individually, remaining with accuracy equal to 1 for recall values higher than 0.7 in both cases.

As Fernandez-Robles et al. pointed out [25], the resting time of milling head tools lies between 5 and 30 minutes. Our experiments, ran on a computer with an i7 processor and 16GB RAM using MATLAB, showed that it takes about 60 seconds to describe the full insert dataset and less than 0.1 seconds to classify all the training data, so the implementation reaches real time performing on a production environment.

5 Tool Wear Classification Based on the Wear Region Size

In this section, we evaluate the classification accuracy obtained using the wear size (area in mm^2). As in the previous experiment, we assess this approach on the Insert-C, Insert-I datasets and also on both together. In order to carry out a fair comparison with the results of our previous experiments, the classification stage was performed using a SVM with intersection kernel and following stratified 10-fold cross validation.

Fig. 14 shows the classification accuracy for the L-H and L-M-H scenarios compared with those obtained with the B-ORCHIZ descriptor. In both experiments B-ORCHIZ achieves the best performance. In the L-H classification,

the best result was obtained in the Insert-I with an accuracy of 88.46% against 85.71% achieved with the simple area descriptor which involves a 3.21% of accuracy increment. In the three classification setting the difference between these two approaches increases significantly. For the Insert-C dataset, B-ORCHIZ improvement reaches 23.35%. However, the highest difference appear when the experiments run on the full dataset (Inserts). The high difference of size between the complete edges and the incomplete ones makes the classification based on the area very poor with just a 61.63% of accuracy in the L-M-H dataset and less than 80% in L-H compared with the 80.24% and 87.06% achieved by our shape descriptor.

These results demonstrate the fact that the area information is not enough to describe precisely the wear level. Techniques based on shape description appear to be a better option to assess the wear level of the inserts.

6 Shape Descriptor Evaluation based on Clustering

In this section, the shape descriptors analyzed in this work are assessed with regard to its power to cluster wear images into homogeneous groups.

6.1 Dendrogram analysis

A dendrogram is a tree-structured graph that represents the result of a hierarchical clustering as the distance between the different clusters. In problems where the number of clusters is not fixed or when the goal is to discern between different sub-clusters within each class, the dendrogram may improve the capacity of taking correct decisions. In addition, dendrograms give specific information about the correlation between the clusters: highly correlated groups are near the bottom of the graph, whilst as we move up the graph the clusters are bigger and the distance between them increases.

6.2 Automatic clustering for Insert dataset

We carried out an automatic hierarchical clustering to compare the groups obtained with the ground truth generated by the expert. The clustering was based on a hierarchical cluster tree using Ward linkage method [26]. This analysis was conducted for each of the three evaluated descriptors, i.e. ZMEG, aZIBO and B-ORCHIZ and for the whole Insert dataset and the Insert-C and Insert-I subsets. The dendograms which represent these clusterings are depicted in Fig. 15.

Our goal is to identify two and three classes within all the wear images. A higher distance determines more separated clusters and therefore, a clearer distinction of whether an insert is damaged or not. In the Insert-C dataset, the class division has a low distance between classes for all the descriptors. It is near 3200 for two classes and around 2000 for three classes. However, for

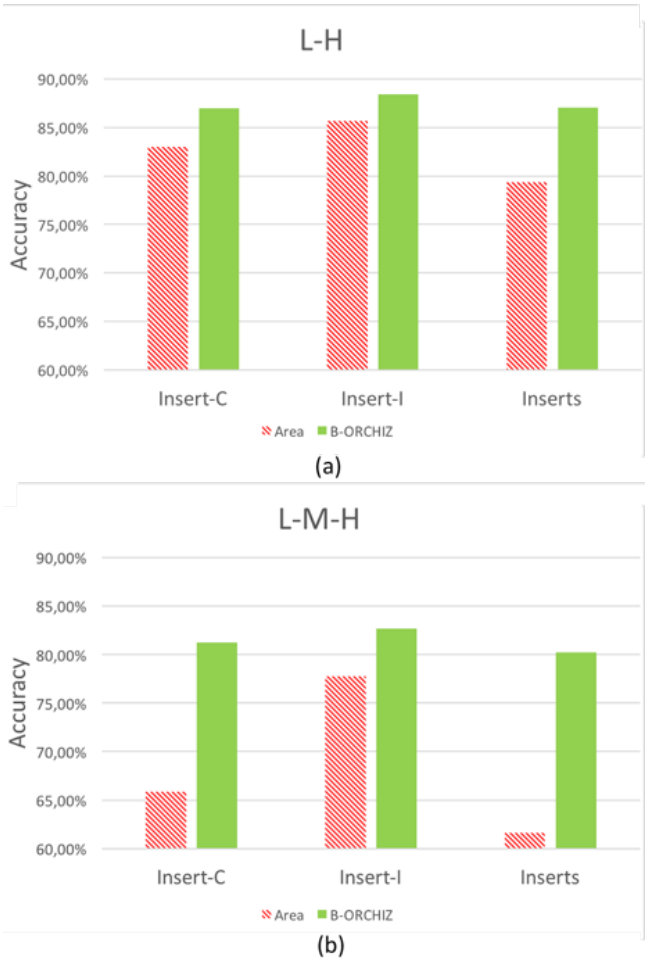

Figure 14: Classification results using B-ORCHIZ descriptor and the wear area size. In (a) the results for L-H experiment. In (b) the results for L-M-H experiment.

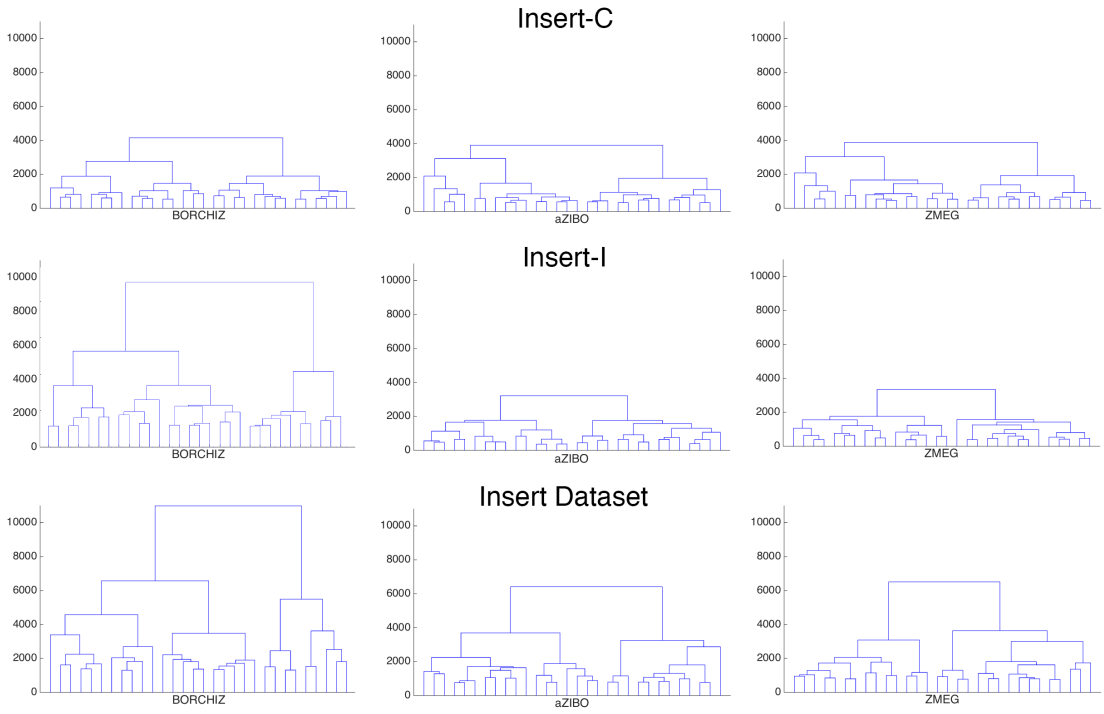

Figure 15: Dendrogram of the clustering obtained using B-ORCHIZ (left), aZIBO (center) and ZMEG(right) descriptors for the Insert dataset and the Insert-C and Insert-I subsets.

the Insert-I subset, the distance between two classes is approximately 6000 with B-ORCHIZ, but just around 2000 with aZIBO and ZMEG. For three classes, the distance between the nearest clusters is around 1500 in both aZIBO and ZMEG and higher than 4000 for the B-ORCHIZ based clustering. This shows that B-ORCHIZ has more discriminant power in the Insert-I subset.

As it is shown in the third row of Fig. 15, the study of the dendogram on the combined set demonstrate that B-ORCHIZ generates descriptors with more discriminant power due to the higher difference between the classes. Ward linkage method ensures very homogeneous classes for the dataset and the dendrogram confirms that, showing a similar distribution of the classes.

According to this analysis, it can be stated that the best group separation is achieved using the proposed B-ORCHIZ method to describe the wear regions.

7 Representative shape of wear classes

7.1 Average greyscale image

After the automatic labelling process using ZMEG, aZIBO and B-ORCHIZ descriptors, we have carried out an evaluation of all the images that, according to the clustering process, belong to the same class in order to extract a representative shape for each one.

Firstly, all the edges have been aligned to the center of the image. For the Insert-C subset, this process consists simply on translating the region of the edge vertically so that its central row is in the middle row of the image. In the case of the Insert-I subset, the left and right edges have different orientations depending on the insert (see Fig. 11(c)). Therefore, before translating them to the middle of the image we have to rotate all the incomplete regions to place them perfectly vertical.

Secondly, all the images have been resized to fixed dimensions and the element-wise sum for all the pixels of every image has been carried out. As we have binary images, if the resulting image has a pixel with value t, it means that t images have wear information on that position.

Finally, the resulting image is averaged and is shown as a grayscale image.

With that representative image for each cluster, we are trying to improve the comprehension of the wear edge classification and give a clue to human experts about the estimated shape of each one.

In Fig. 16 we can see the representative images for the three level clasification for the Insert-C subset. While aZIBO and ZMEG show very similar representative images, the B-ORCHIZ high wear prototype is very different: B-ORCHIZ shows a larger wear area, what can be interpreted as the reason to make possible the best classification of that kind of images, allowing only images with high wear to be clustered together and leaving the rest for the medium or low wear cluster.

The same happens with the Insert-I subset where the difference between classes using B-ORCHIZ is higher than using the grouping provided by the

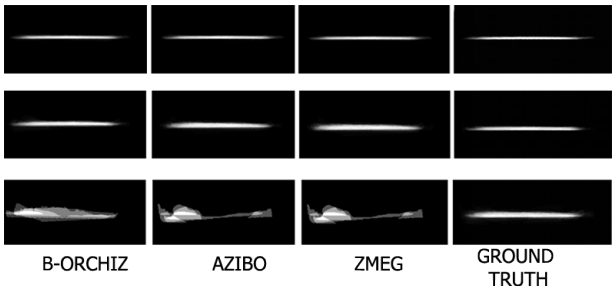

Figure 16: Representative images for three level of wear (L: first row, M: second row and H: third row) for the Insert-C subset using clustering. Insert wear described with B-ORCHIZ, aZIBO and ZMEG with its associated ground truth (columns from left to right) for automatic clustering. Images are aligned and the average value of each pixel of the image representing the gray level of the representative image is calculated.

expert.

Based on this study, we can conclude that the descriptor that better represents the different edge wear is B-ORCHIZ because it provides more information about the wear region shape than the others descriptors and the expert clustering, being quite useful to study the wear process, to train new personal and to generate automatic templates.

7.2 3D Representation and contour map

In this section, we show with more detail the representative shape for each subset of the dataset (Insert-C and Insert-I) depending on the wear level. We focus on B-ORCHIZ to obtain the representative image for each class because, as we pointed out in the previous subsection, B-ORCHIZ offers more information about the shape depending on the wear level. Fig. 17 depicts the representative images for the Insert-C and Insert-I when we consider two wear classes. In Fig. 18, the representative images for the three classes are shown. These images demonstrate that the shape of the wear region can clearly offer reliable information about the insert state.

In general, the L-H labelling offers less information than the L-M-H one. Using the L-M-H labelling, L and M classes are quite similar in terms of shape but in the case of the H class, the shape is really irregular and the surface is bigger than in the other cases. It is also remarkable that, for the Insert-I dataset with low wear, the insert is more worn when it is closer to the cutting surface. Thus, the shape of the wear region can clearly offer reliable information about the state of the insert.

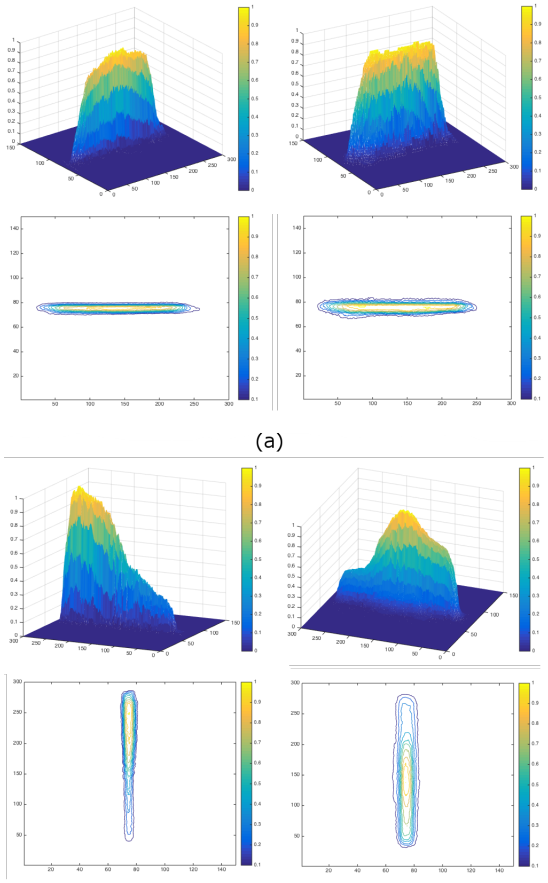

Figure 17: Representative images for (a) the Insert-C subset and (b) the Insert-I subset, L-H labelling (from left to right). First row represents the surface and second row represents the contour for the plan view.

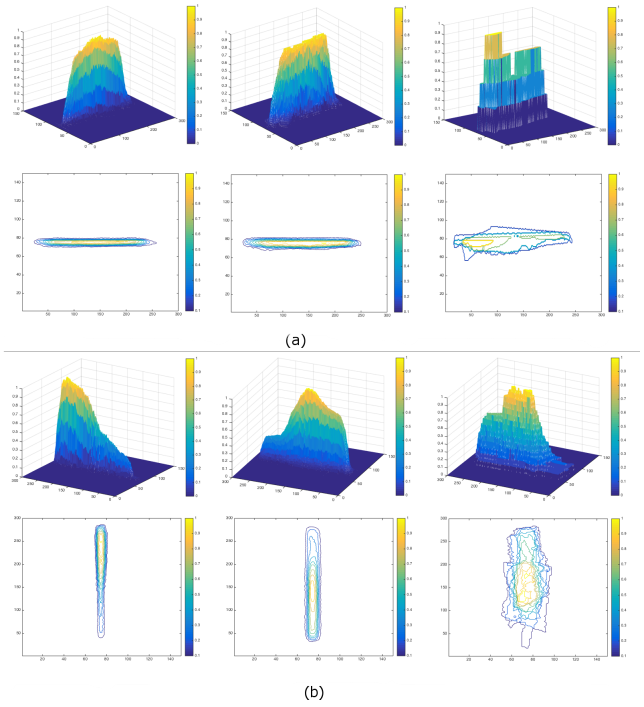

Figure 18: Representative images for (a) the Insert-C subset and (b) the Insert-I subset, L-M-H labelling (from left to right). First row represents the surface and second row represents the contour for the plan view.

8 Conclusions

In this paper, we present a new approach to monitor tool wear in edge profile milling operations using computer vision. Our aim is to classify the insert according to its wear stage as a function of the wear region shape with a machine learning classification model. To achieve this goal, we propose B-ORCHIZ, a new shape descriptor computed from the tool image that captures both, global and local image information, and guarantees total invariance to rotation.

In order to assess this proposal, we created a dataset with images from 53 tools (with four cutting edges each one) that was labelled by an expert into two and three wear classes.

Following a supervised learning approach, the performance of a SVM classifier in terms of classification accuracy is assessed on the Insert dataset comparing B-ORCHIZ with other two descriptors: ZMEG and aZIBO. B-ORCHIZ outperformed the other methods in the scenarios evaluated. The experiments demonstrate that the incomplete edges achieve better performance for the wear classification than the complete ones. The main reason is that the Insert-I dataset wear is focused in the corners which is where the wear is more relevant.

Furthermore, a comparision between B-ORCHIZ proposal and the descriptor based on the size of the wear has been performed demonstrating that the shape based one discriminate better between the different wear level.

Additionally, a cluster analysis shows that B-ORCHIZ has more discrimination power to separate the tool wear images into homogeneous groups and it provides more detailed information of the wear region states.

These results show that computer vision techniques can be taken into account for future real projects as a reliable approach that enables tool condition monitoring in edge profile milling operations. Evaluating this approach on end milling or face milling is part of our future work.

Acknowledgements

This work has been supported by the reseach project with ref. DPI2012- 36166 from the Spanish Ministry of Economy and Competitiveness and the PIRTU program of the Regional Government of Castilla y León. Dr. Gonzlez-Castro is funded by the Row Fogo Charitable Trust (Grant No. R43412).

References

References

[1] M. Malekian, S. S. Park, M. B. Jun, Tool wear monitoring of micro-milling operations, Journal of Materials Processing Technology 209 (2009) 4903 – 4914.

[2] G. Wang, Y. Yang, Q. Xie, Y. Zhang, Force based tool wear monitoring system for milling process based on relevance vector machine, Advances in Engineering Software 71 (2014) 46 – 51.

[3] A. Azmi, Monitoring of tool wear using measured machining forces and neuro-fuzzy modelling approaches during machining of GFRP composites, Advances in Engineering Software 82 (2015) 53 – 64.

[4] B. Kaya, C. Oysu, H. M. Ertunc, Force-torque based on-line tool wear estimation system for CNC milling of inconel 718 using neural networks, Advances in Engineering Software 42 (2011) 76 – 84.

[5] X. Li, A brief review: acoustic emission method for tool wear monitoring during turning, International Journal of Machine Tools and Manufacture 42 (2002) 157 – 165.

[6] K. V. Rao, B. Murthy, N. M. Rao, Prediction of cutting tool wear, surface roughness and vibration of work piece in boring of AISI 316 steel with artificial neural network, Measurement 51 (2014) 63 – 70.

[7] C. Scheffer, P. Heyns, Wear monitoring in turning operations using vibration and strain measurements, Mechanical Systems and Signal Processing 15 (2001) 1185 – 1202.

[8] J. Loizou, W. Tian, J. Robertson, J. Camelio, Automated wear characterization for broaching tools based on machine vision systems, Journal of Manufacturing Systems 37, Part 2 (2015) 558 – 563.

[9] S. Kurada, C. Bradley, A review of machine vision sensors for tool condition monitoring, Computers in Industry 34 (1997) 55 – 72.

[10] S. Dutta, S. Pal, S. Mukhopadhyay, R. Sen, Application of digital image processing in tool condition monitoring: A review, CIRP Journal of Manufacturing Science and Technology 6 (2013) 212 – 232.

[11] C. Zhang, J. Zhang, On-line tool wear measurement for ball-end milling cutter based on machine vision, Computers in Industry 64 (2013) 708 – 719.

[12] Y. Chethan, H. Ravindra, Y. K. Gowda, G. M. Kumar, Parametric optimization in drilling en-8 tool steel and drill wear monitoring using machine vision applied with taguchi method, Procedia Materials Science 5 (2014) 1442 – 1449. International Conference on Advances in Manufacturing and Materials Engineering, ICAMME 2014.

[13] A. Datta, S. Dutta, S. Pal, R. Sen, Progressive cutting tool wear detection from machined surface images using voronoi tessellation method, Journal of Materials Processing Technology 213 (2013) 2339 – 2349.

[14] S. Dutta, S. K. Pal, R. Sen, Progressive tool flank wear monitoring by applying discrete wavelet transform on turned surface images, Measurement 77 (2016) 388 – 401.

[15] X. Shu, X.-J. Wu, A novel contour descriptor for 2d shape matching and its application to image retrieval, Image and Vision Computing 29 (2011) 286 – 294.

[16] N. Laiche, S. Larabi, F. Ladraa, A. Khadraoui, Curve normalization for shape retrieval, Signal Processing: Image Communication 29 (2014) 556 – 571.

[17] J. Barreiro, M. Castejón, E. Alegre, L. Hernández, Use of descriptors based on moments from digital images for tool wear monitoring, International Journal of Machine Tools and Manufacture 48 (2008) 1005 – 1013.

[18] C. Singh, Pooja, An effective image retrieval using the fusion of global and local transforms based features, Optics & Laser Technology 44 (2012) 2249–2259.

[19] F. M. Anuar, R. Setchi, Y. kun Lai, Trademark image retrieval using an integrated shape descriptor, Expert Systems with Applications 40 (2013) 105 – 121.

[20] O. García-Olalla, E. Alegre, L. Fernández-Robles, P. Malm, E. Bengtsson, Acrosome integrity assessment of boar spermatozoa images using an early fusion of texture and contour descriptors, Computer methods and programs in biomedicine 120 (2015) 49–64.

[21] M. García-Ordás, E. Alegre, V. González-Castro, D. García-Ordás, aZIBO: A New Descriptor Based in Shape Moments and Rotational Invariant Features, in: Pattern Recognition (ICPR), 2014 22nd International Conference on, 2014, pp. 2395–2400. doi:10.1109/ICPR.2014.415.

[22] G. Zhang, S. To, G. Xiao, Novel tool wear monitoring method in ultra-precision raster milling using cutting chips, Precision Engineering 38 (2014) 555 – 560.

[23] N. Cadorin, R. Zitoune, Wear signature on hole defects as a function of cutting tool material for drilling 3d interlock composite, Wear 332333 (2015) 742 – 751. 20th Intenational Conference on Wear Materials.

[24] S. Belongie, J. Malik, J. Puzicha, Shape matching and object recognition using shape contexts, IEEE Transactions on Pattern Analysis and Machine Intelligence 24 (2001) 509–522.

[25] L. Fernández-Robles, G. Azzopardi, E. Alegre, N. Petkov, Cutting Edge Localisation in an Edge Profile Milling Head, Springer International Publishing, Cham, 2015, pp. 336–347.

[26] J. H. Ward, Hierarchical grouping to optimize an objective function, Journal of the American Statistical Association 58 (1963) 236–244.